J Nanostruct 12(2): 303-315, Spring 2022

RESEARCH PAPER

Eco Friendly Synthesis of Zinc Oxide Nanoparticles and Printing onto Electrically Conductive Substrate Using Electrostatic Spray Deposition

Maryam Karimi [1], Seyed Mohammad Mirkazemi [1], Yaser Vahidshad [2], Jafar Javadpour [1]*

[1] School of Metallurgy and Materials Engineering, Iran University of Science & Technology, Narmak, Tehran, Iran

[2] Space Transportation Research Institute, Iranian Space Research Center, Fath Highway, Tehran, Iran

ARTICLE INFO

Article History:
Received 05 December 2021
Accepted 07 March 2022
Published 01 April 2022

Keywords:
Electrostatic spray deposition
Semiconductor thin films
Thermolysis
Zinc oxide nanoparticle

ABSTRACT

The study presents the efficient synthesis of hexagonal wurtzite zinc oxide (ZnO) nanoparticles and a stable nano colloid by a one-pot thermolysis synthesis method. In this investigation, the average particle size for the synthesized ZnO was about 60 nm, condensed and adhesive zinc oxide thin films were productively sprayed onto fluorine doped tin oxide glass at room temperatures using a controllable electrostatic spray deposition method. This technique is useful method to deposit a facile, non-vacuum, and inexpensive layer. The synthesized nanoparticles were characterized by X-ray diffraction, dynamic light scattering, Fourier-transform infrared spectroscopy, and purity and surface morphology of thin film was confirmed by scanning electron microscope. Thermogravimetric analysis of the ZnO nanoparticles showed that weight loss continued until 450 ˚C. Results revealed optimized deposition conditions at the voltage of 26 kV, the flow rate of 3 µl/min, and nozzle to substrate distance of 8 cm. In the wavelength ranging between 300-900 nm, the optical absorbance and transmittance measurements were recorded and the UV–Visible spectrum of the ZnO thin film showed maximum absorbance at around 350 nm.

How to cite this article
Karimi M., Mirkazemi S M., Vahidshad Y., Javadpour J. Eco Friendly Synthesis of Zinc Oxide Nanoparticles and Printing onto Electrically Conductive Substrate Using Electrostatic Spray Deposition. J Nanostruct, 2022; 12(2):303-315. DOI: 10.22052/JNS.2022.02.008

INTRODUCTION

Zinc oxide (ZnO) is a viable semiconductor compound due to its unique piezoelectric and transparent conducting properties along with high conductivity and better transparency in the visible region, making it a versatile substance. [1]. In addition, ZnO has a wide band gap (3.37 eV) at room temperature and a large exciton binding energy (60 meV), low toxicity, cost-effective, and high conductivity [2-6]. ZnO is an ideal candidate in many energy conversion and optoelectronics applications such as photovoltaics, laser diodes, photo-electrocatalytic, water oxidation, and photocatalytic degradation of organic dyes [7-9].

For solar cell applications, various transparent conducting oxides (TCOs) have been identified and utilized over the years due to their suitability. However, the most frequent oxides in the PV area are TCOs, ZnO [10], Indium tin oxide (ITO) [11], and SnO2 [12]. ZnO is considered the most effective TCO material due to its properties and cost-friendly [13]. Further, for the fabrication

* *Corresponding Author Email: y.vahidshad@isrc.ac.ir*

of ZnO films, several deposition techniques have been successfully employed such as spray pyrolysis [14, 15], chemical bath deposition (CVD) [16], and RF sputtering [17] atomic layer deposition [18]. However, in the past few years, the electrostatic spray deposition (ESD) technique has emerged as a leading method for preparing a variety of functional metal oxide thin films [19-24]. Electrostatic spray coating (ESC) is efficient in the deposition of nanoparticles due to its uniqueness to uniformly charge particles with the same electric polarity, which repels the particles and reduces the chances to form clusters. In addition, ESC offers the benefits of depositing on large surfaces, coating parts with complex geometries, high deposition rate, and can be easily scaled up [25]. In this fabrication technique, the morphology and thickness of the deposited layers can be facilely controlled [26, 27].

Electrostatic spray deposition is more advantageous than other conventional mechanical atomizers because of the smaller size of the droplets that can be in range of nanometers. The standard deviation of droplets size helps the formation of uniform layers. Additionally, due to electrical repulsion, the charged droplets are self-dispersing and resulting in the reduction of coagulation. With the help of electric field gradients, the flow of charged droplets can be focused/dispersed on the substrate. As a result, the deposition capacity of charged spray is higher than uncharged droplets such as spin coating, hence, the waste of raw materials will be reduced. Another benefit of ESD is its lower cost than chemical vapor deposition, physical vapor deposition, and sputtering [28, 29]. Similarly, the formation of droplet or spray size obtained using the ESD technique is smaller than other atomization methods which results in a narrower size distribution [30] due to its unipolar charged properties and devoid of aggregation. On the other hand, the relative growth rate of the thin film using ESD is higher than other techniques i.e. CVD or Physical Vapor Deposition (PVD) [28]. This method is also highly reproducible due to the absence of a vacuum apparatus which otherwise can cover a large area [31].

The direct heating of the substrates is one of the main drawbacks of the ESD technique because a set up to heat large substrates consumes more energy, hence decreasing its overall energy efficiency [32]. Further, many researchers deposited ZnO films using EDS in which the substrate's temperature was recorded as more than 300 ˚C [33-36]. Consequently, due to the heating of the substrate, it has to endure high-temperature deposition processes, while depositing thin films at lower temperatures ensures the maintenance of substrate at a low temperature making its usage possible as a flexible substrate [37].

In the present study, an effective and economically viable technique for the fabrication of ZnO thin film at room temperature is investigated. In the precursor solution, because of some limitations on controlling the stoichiometry and high deposition temperatures, a stabled nano colloid was employed for the deposition process. In such studies, the substrate heated up to 400-500 °C. Furthermore, when the heating temperature exceeds 400 °C, oxidation of the film increases in an open atmosphere. Additionally, in this process, green and polar solvents i.e. polyol solvents which are considered green, biocompatible, biodegradable, and sustainable substances, were used to synthesize ZnO nanoparticles by the thermolysis method. In like manner, these solvents allow for excellent control of particle size, size distribution, and agglomeration [38]. In the next step, ethanol was used to prepare nano-colloids by stabilizing nanoparticles in this polar media, while Chen et al. claimed it is difficult to obtain nanostructured thin films by ESD using an alcoholic solution [39]. This high vapor pressure solvent (ethanol) could evaporate at room temperature that is cost-effective and controllable in larger scales or industrial sections. Hence, to achieve this objective, the colloid of nanoparticles was sprayed onto the electrically conductive substrate, which provides a polar interface between ZnO and the substrate to overcome the use of extreme heat during the process with aid of green and low toxic solvents.

MATERIALS AND METHODS

ZnO nanoparticles were synthesized by mixing zinc acetate dihydrate ($Zn(O_2CCH_3)_2(H_2O)_2$, Ethylene glycol (EG) $(CH_2OH)_2$, 99 %) as the solvent, and polyvinylpyrrolidone (PVP) $((C_6H_9NO)_n$, 99.99 %) as the surfactant. Zinc acetate (1.75 mmol) was dissolved in 20 ml of EG with 2% w/v PVP for about 15 minutes at room temperature. In the next step, the transparent solution was stirred at 60 ˚C for 1 hour to form Zinc acetate-PVP complex. With a heating rate of 5 ˚C/min, the solution was heated up to 150 ˚C and was kept for an hour at

Table 1. ZnO thin films deposition conditions by EDS

Sample	Distance (mm)	Voltage (kV)	Flow rate (µl/min)
ZO-L1	80	26	3
ZO-L2	80	28	3
ZO-L3	80	24	3
ZO-L4	80	26	2
ZO-L5	80	26	1
ZO-L6	60	26	3
ZO-L7	100	26	3

this temperature.

For the preparation of nano-colloid, 0.0375 g of synthesized nanoparticles dispersed in 10 ml of ethanol. Then the ultrasonication was used for 4 hours to reduce the agglomeration of the nanoparticles. The ZnO nano-colloid was deposited by the electrostatic spray deposition process onto an FTO glass substrate at room temperature (Table 1) for 30 minutes. At 500 ˚C, the thin films were annealed for 30 minutes after the deposition.

Powder X-ray diffraction (XRD) was performed on a GNR X-Ray Explorer with the use of Cu-Kα (1.541 Å) radiation. Dynamic light scattering (DLS) experiment was conducted on Malvern Zetasizer ZS-ZEN3600 red badge. FTIR spectra were conducted Nicolet 6700 FT-IR spectrometers from Thermo scientific. Thermogravimetric analysis (TGA) of ZnO nanoparticles was carried out by using Linseis TGA PT1600. The microstructures and morphologies of the deposited thin films were studied using the TESCAN Vega Model scanning electron microscope. The optical properties of the studied films were determined at room temperature, using a Shimadzu UV-2550 spectrometer. A clean glass substrate was used as a reference for absorption measurements.

RESULTS AND DISCUSSION

Fig. 1. Shows the XRD pattern of synthesized ZnO nanoparticles, which clearly depicts that the hexagonal wurtzite structure with all the diffraction peaks of the formed ZnO nanoparticles can be indexed. It well matches the standard JCPDS Card No. 1-1136 [40]. It is important to note that in the XRD pattern of the synthesized ZnO nanoparticles no impurity phase was detected when this spectrum was compared with the ZnO reference card [41]. The purity of the sample was indicated owing to high sharp intensities in the diffraction pattern and the presence of Miller

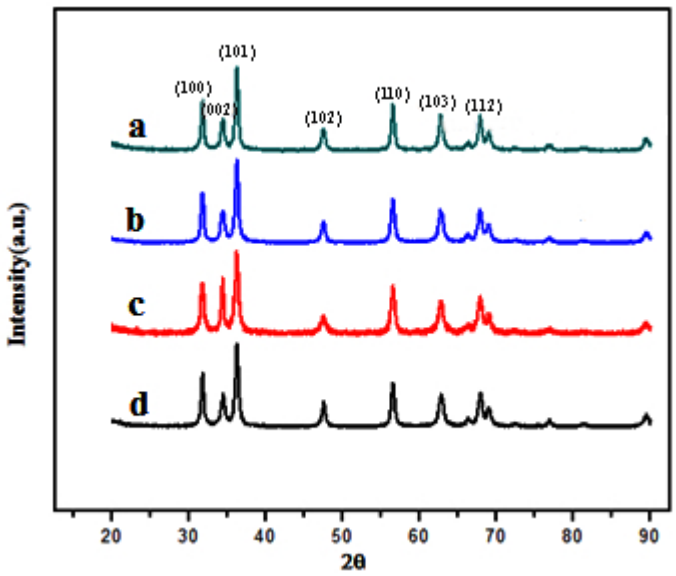

Fig. 1. X-ray diffraction patterns of ZnO nanoparticles (a) Non PVP (b) 0.5% w/v PVP (c) 1% w/v PVP (d) 2% w/v PVP

indices (100), (002) and, (101) [42].

Debye–Scherrer's equation 1 [43] was used to calculate the average size of crystallite. The normal crystallite dimensions of ZnO were found at the approximate range of 17 nm from the above calculations.

$$D = \mathrm{K}\lambda/\mathrm{B}\cos\theta \quad (1)$$

D is the crystallite size, k is the crystallite-shape factor (0.9), λ depicts the X-ray wavelength of 1.5421 Å, β and refer to the width (full-width at half-maximum) of the X-ray diffraction peak in radians and θ is the Bragg's angle.

To study the morphology of ZnO nanoparticles, the concentration of PVP is changed. PVP, due to the strong interaction between the O and N atoms in the pyrrolidone and surface of nanoparticles is used as a capping agent [41]. The product sizes and morphologies are impacted by the presence of PVP on different crystallographic planes of nanocrystals [44]. With the increase of PVP on various crystallographic surfaces, a shell forms by PVP around the particles which prevent their aggregation and subsequent increase in size, the diameter of ZnO nanoparticle is reduced because the growth units cannot be deposited on the crystallographic surfaces [45]. The orbitals of the metal ions may be occupied by the polar group of PVP. Further, as the PVP and Zn^{+2} form a coordinate bond, hence diminishing the concentration of Zn^{+2} and smaller crystal sizes are obtained [46].

The steric effect of PVP covers the surface of the ZnO nanoparticles via physical and chemical bonds restricting particle-particle contact that prevents agglomeration of nanoparticles inside the spherical aggregates [47].

Fig. 2. shows a structural model for PVP-capped ZnO nanoparticles, the structural models and the orientation are significant factors in determining the conditions under which a stable nano-colloid can be obtained. Three different conditions have been considered to understand the importance of capping agent amounts to prepare a stable colloid. Firstly, in Fig. 2a it observed that in the presence of lesser amounts of capping agent, it would not prevent the ZnO nanoparticles agglomeration because the coating of PVP is not sufficient to rise steric stabilization. According to Fig. 2b to obtain a stable colloid and raise repulsive force between the surfaces the optimum concentration of PVP is required while more than the optimum amount (Fig. 2c) can cause the attraction among their polymeric chains due to the osmotic pressure difference [48].

In this study, the sample with 2% w/v PVP was the most stable colloid because this nano-colloid showed no participation after 21 days based on the observation method. Therefore, the colloid in

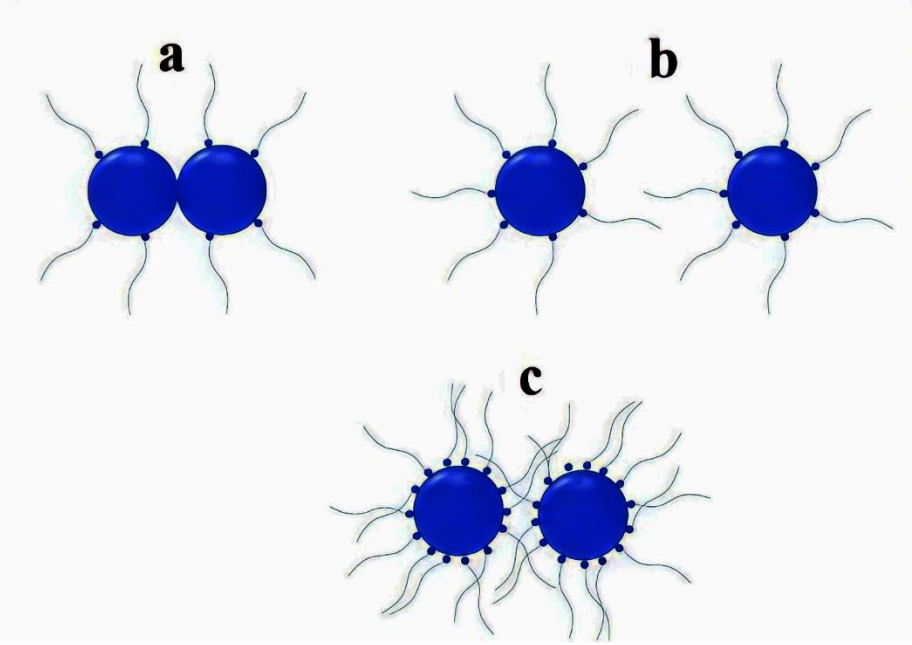

Fig. 2. Structural model for PVP-capped ZnO nanoparticles (a) lower amount of PVP (b) optimum amount of PVP (c) more than the optimum amount of PVP

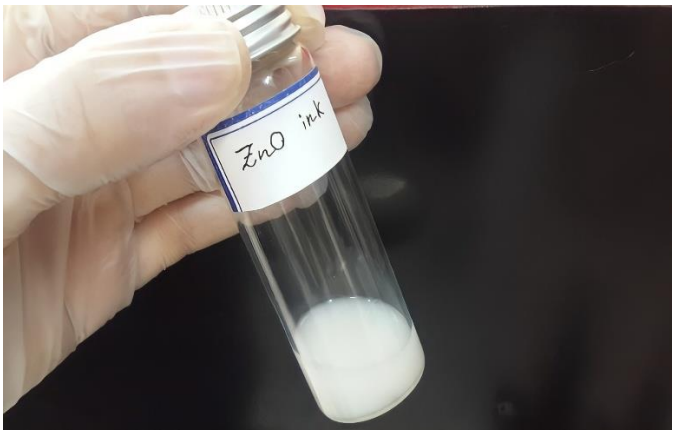

Fig. 3. Colloidal ink of ZnO nanoparticles in ethanol after 21 days

Fig. 3. is used in the deposition process.

A particle size analyzer was used for obtaining the particle size distribution and the average size of zinc oxide nanoparticles. Fig.4. shows the result for the ZnO nanoparticles sample obtained by DLS According to the graph, at a synthesis temperature of 150 ˚C, the average particle size for the synthesized ZnO was about 60 nm, as shown in Fig. 4. The sizes of the nanoparticles ranged between 50-70 nm.

There are two possibilities based on the calculation of the particle size of ZnO samples using DLS. Firstly, the size of ZnO nanoparticles even after agglomeration was small enough to be in the range of 60 nm. Secondly, the aggregation of nanoparticles prevented by the steric hindrance effect of PVP and stabilized to remain in nano sized.

The size calculated by the DLS test known as hydrodynamic diameter shows the particle's size in the surrounding dispersant. The Stokes-Einstein equation was used to calculate the size of the particle [49]:

$$d(H) = {}^{kT}/_{3\pi\eta D} \quad (2)$$

Where: d(H) = hydrodynamic diameter
T= absolute temperature
η= viscosity
D= translational diffusion coefficient

Hydrodynamic diameter value is dependent on the particle core, surface modifications to the particle and the surrounding ions present in the

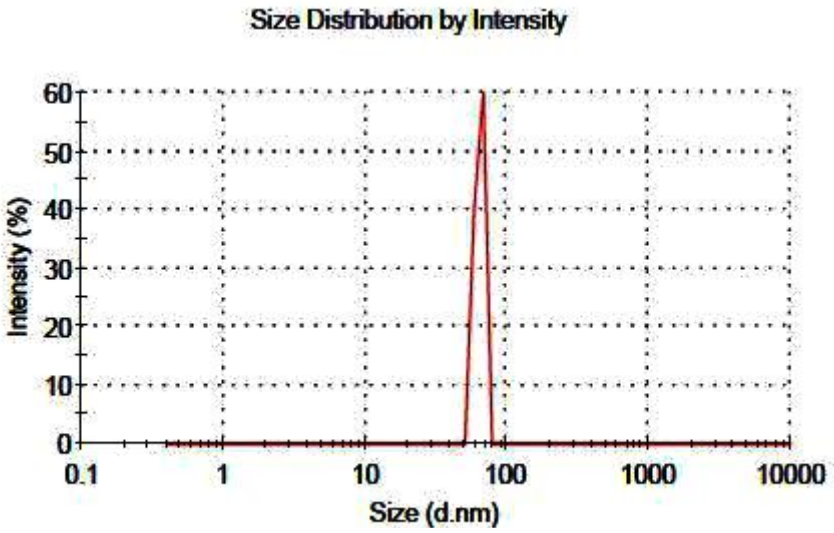

Fig. 4. Spectrum of size distribution of ZnO nanoparticles in ethanol media by DLS technique

solvent Apart from hydrodynamic diameter and PVP-capped ZnO nanoparticles, the reported ZnO nanoparticles size in this technique is larger due to the bias of the technique toward the measurement of larger particles (or even aggregates). [49-51]. As shown in the Stokes-Einstein equation in low viscosity solvents such as ethanol hydrodynamic diameter will be increased.

The FTIR spectra of ZnO nanoparticles in Fig. 5. and Table 2 shows absorption peaks at 3388, 2926 cm^{-1} could be appointed to hydroxyl (OH) groups and CH_2 vibration modes of residue EG, not completely removed after the washing procedure [52], 1292 is related to CH_2 wagging and C–N stretching peaks of PVP and 1590 cm^{-1} could correspond to the C=O stretch of PVP [53, 54]. Moreover, the medium to weak bands for pure ZnO at ZnO polymeric hybrid at 889 cm^{-1} are assigned to the vibrational frequencies due to the change in the microstructural Zn–O lattice. For the presence of C–O, and C–H vibration modes of PVP the peaks were sited at 1050 cm^{-1} and 1092 cm^{-1} for ZnO, which acts as a capping agent in the synthesis of nano zinc oxide. The remaining peaks around 1661 cm^{-1} and 1423 cm^{-1} for ZnO characteristic peaks are as a result of polymeric O–H stretching vibration of the H_2O small amount inside the ZnO nanocrystals [55-57].

The decomposition in the pure PVP can be categorized and divided into two stages. Evident from the differential thermal gravimetric (DTG) Curve shown in Fig. 6. First, one with slight weight loss and lies between 30 and 100 °C can attribute to the evaporation of physically trapped moisture [58, 59]. The burning of organic species present in the precursor powders (organic mass remained from PVP) and the thermal events associated with the chemically bound water which corresponds to a 28% weight loss in the second step shows a significant weight loss that takes place from 100 to 450 °C. Above 500 °C, no further loss in weight and no significant thermal effect were observed, which means that any higher temperature prevents further decomposition [60].

The UV–visible absorbance spectrum is an important technique to evaluate the optical

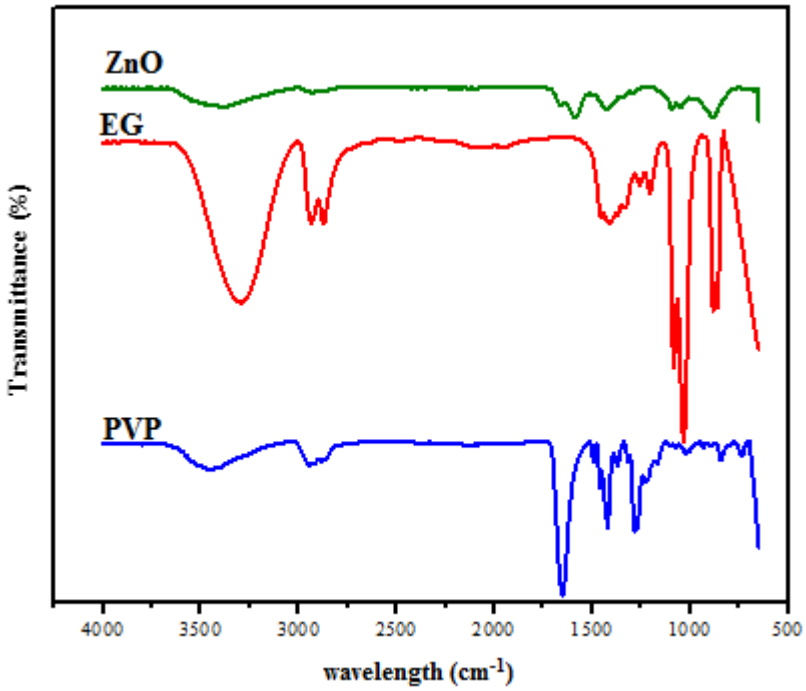

Fig. 5. FT-IR spectrum of the ZnO nanoparticles, Ethylene glycol and polyvinylpyrrolidone

Table 2. FTIR peaks for ZnO nanoparticles, Ethylene glycol and polyvinylpyrrolidone

ZnO nanoparticles (cm^{-1})	3388	2926	1661	1590	1423	1292	1092	1050	888
EG (cm^{-1})	3299	2936	2873	1412	1204	1083	1032	881	861
PVP (cm^{-1})	3441	2948	1650	1492	1460	1421	1316	1284	

properties of the ZnO nanoparticles. Tauc's equation [1] was used to measure the optical band gap energy (Eg) of ZnO for direct bad gap semiconductors:

$$\alpha h\nu = A(h\nu - E_g)^{\frac{1}{2}} \quad (3)$$

Where absorption coefficient is represented by α, hν indicates the incident photon energy, and A is a constant. These properties have shown in Fig. 7. The spectrum indicates a strong absorption band located at 375 nm and the average band gap estimated from the intercept of the linear portion of the (αhν) 2 vs. hν plots on hν axis [61]. By the extrapolation of the straight-line portion of the plot to the zero absorption coefficient, the band gap energy (eV) is obtained. As shown in Fig. 7, the band gap value was found to be ~3.28 eV.

In depositing nano-colloids, the ESD processing

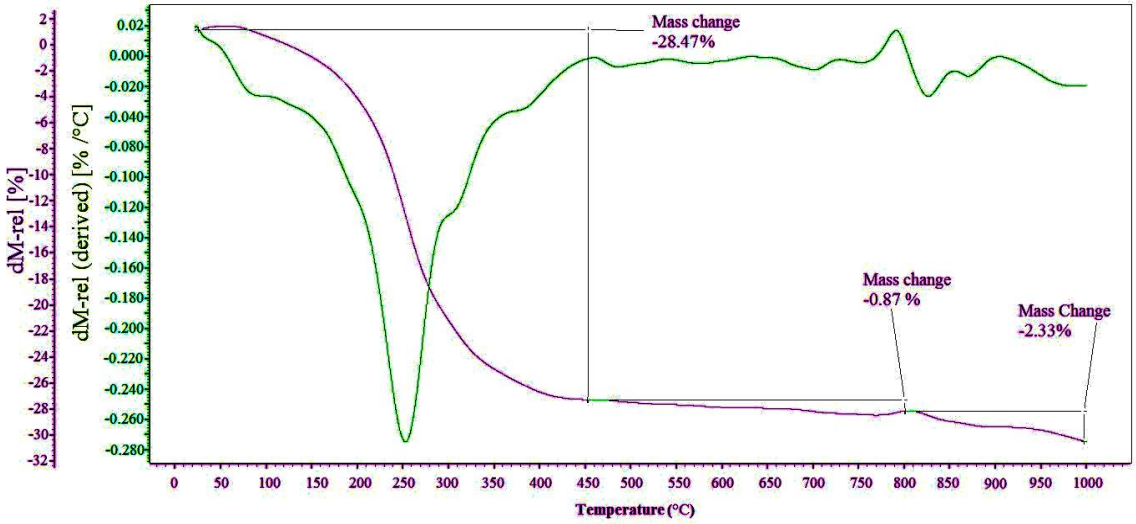

Fig. 6. TG/DTG thermogram of PVP capped ZnO

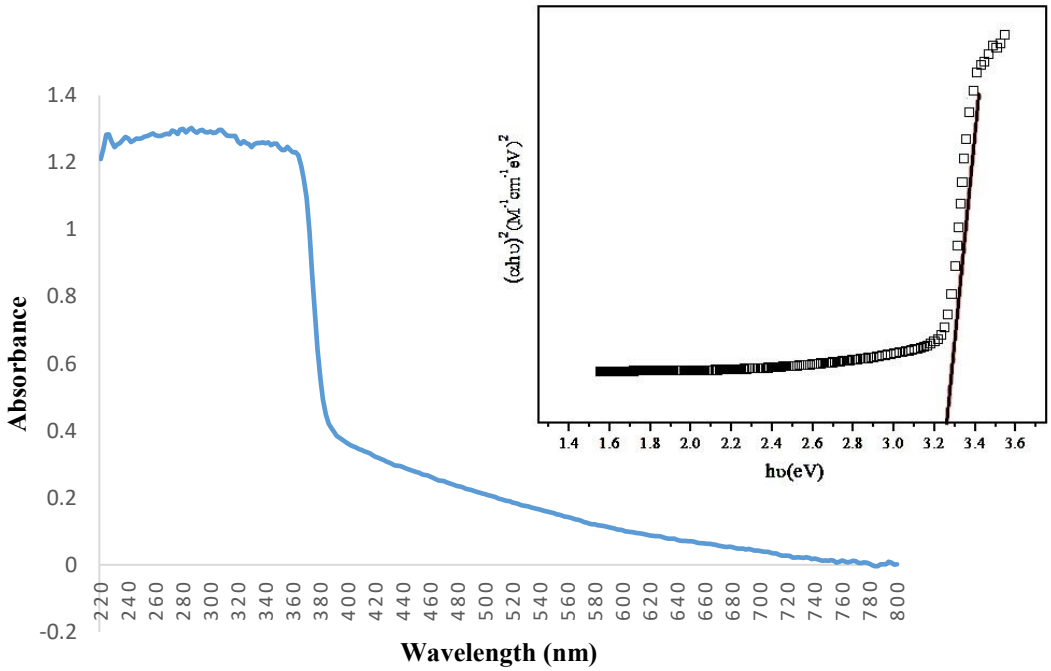

Fig. 7. UV-visible spectrum of ZnO nanoparticles

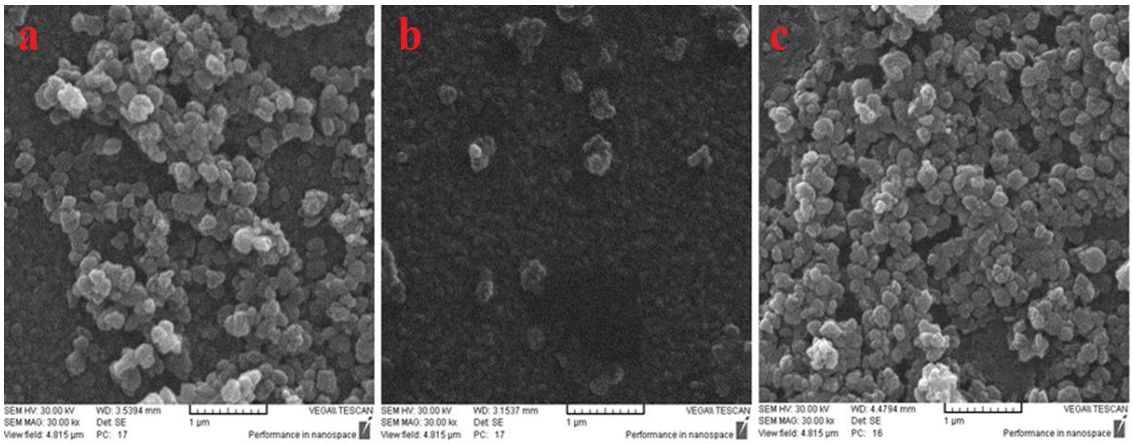

Fig. 8. Morphology of ZnO thin films at flow rate of 3 µl / min, 8 cm distance from the substrate at various voltages (a) ZO-L2 (b) ZO-L1 (c) ZO-L3

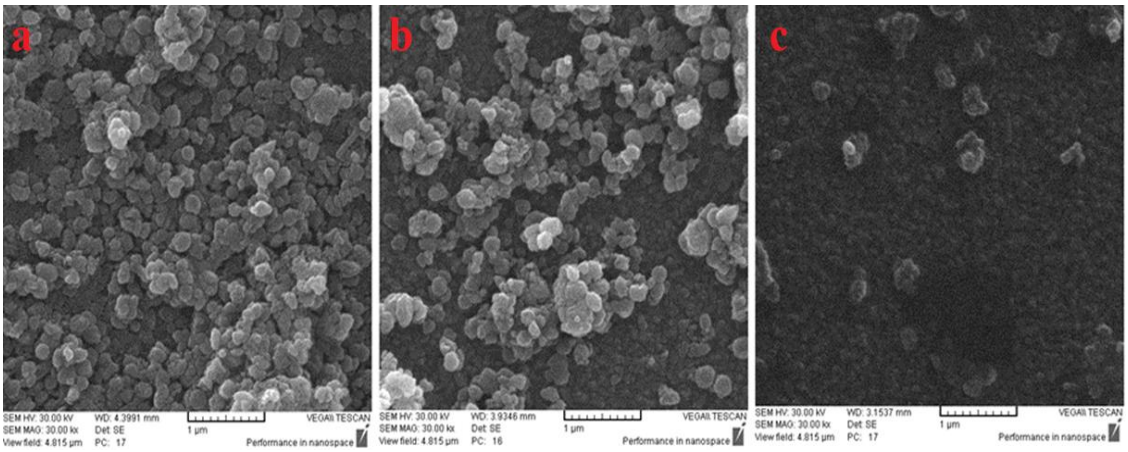

Fig. 9. Morphology of ZnO thin films at voltage of 26 kV, 8 cm distance from the substrate and various flow rates, (a) ZO-L5 (b) ZO-L4 (c) ZO-L1

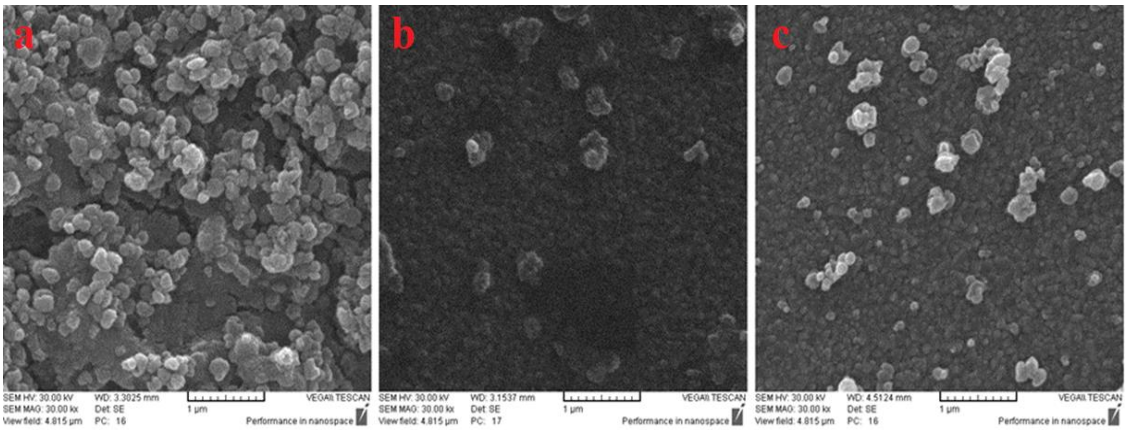

Fig. 10. Morphology of ZnO thin films at the voltage of 26 kV, at a flow rate of 3 µl / min by changing nozzle to substrates distances: (a) ZO-L6 (b) ZO-L1 (c) ZO-L7

parameters have a significant role in thin film formation, the ZnO thin films are prepared at different conditions according to Table 1. based on Fig. 8. At the at a flow rate of 3 µl / min, 8 cm distance from the substrate the SEM image of ZO-L1 showed a relatively smooth surface in comparison with ZO-L2 and ZO-L3, so stable con-jet forms at the voltage of 26 kV, while larger particles were observed on the film surface at the voltages of 24 and 28 kV. As shown in Fig. 9. by increasing the flow rate (ZO-L3>ZO-L4>ZO-L5) from 1 to 3 µl/ min, and keeping other processing parameters constant, at the voltage of 26 kV and nozzle to substrate distance of 8cm, the uniformity of the deposited layers has increased. Fig. 10. indicates increasing the nozzle to substrate distances from 6 cm (ZO-L6) to 8 cm (ZO-L1) decreases agglomeration of particles and crack formation on the surface while increasing this distance from ZO-L1 to 10 cm (ZO-L7) larger particles have formed on the film surface.

Fig. 11. represents energy-dispersive X-ray spectroscopy (EDS) of ZnO thin film. As shown in Fig. 11b, the elements in the deposited thin film were confirmed by EDX. With regards to the atomic mass (Fig. 11a), the elemental composition of Zn, O, Au, and Sn in the thin film was 10%, 65%, 14.18%, and 9.99%, respectively. Gold has been used as a conductive coating of the sample as indicated by the presence of Au in the peak, while the presence of Sn is related to the FTO glass.

Cross sections of ZO-L1 and ZO-L7 are shown in Fig. 12. According to this figure, there is a difference in roughness between ZO-L1 and ZO-

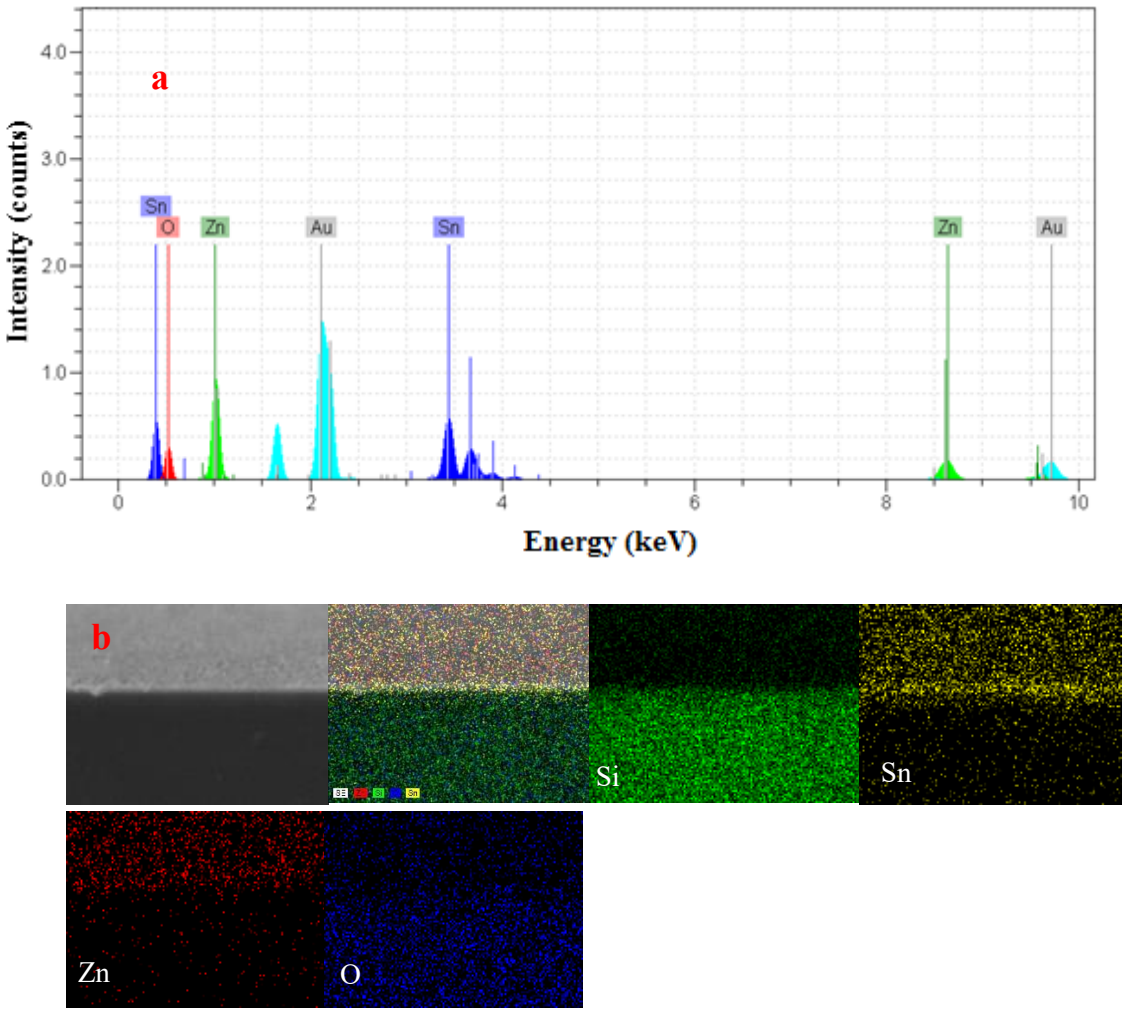

Fig. 11. (a) EDS spectrum (b) elemental mapping images of Si, O, Sn, and Zn elements, of ZO-L1

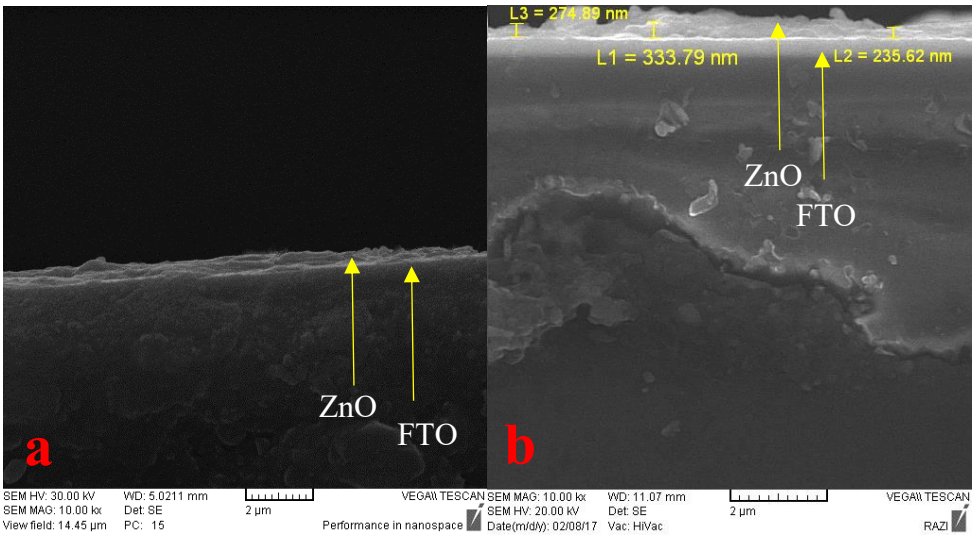

Fig. 12. Cross-sectional micrograph of ZnO thin films (a) ZO-L1 (b) ZO-L7

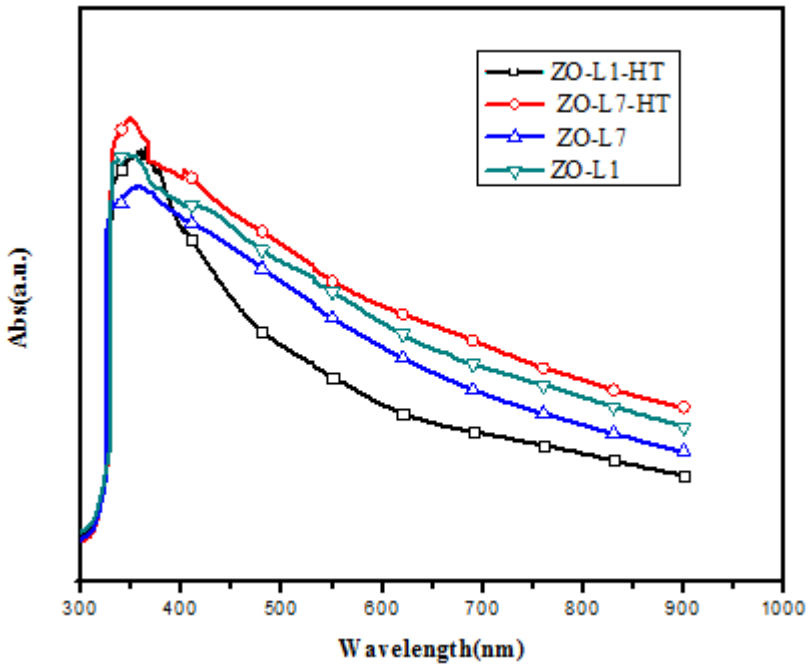

Fig. 13. UV-Vis absorption Spectra of ZO-L1 and ZO-L7 thin films on FTO substrate before and heat treatment heat treatment at 500 ˚C.

L7. It shows that the roughness of ZO-L1 is lower than that of ZO-L7. However, it is observed that the thickness of the deposited thin films is less than 400 nm in both conditions.The spectroscopy features of ZnO nanoparticles were measured using UV–visible absorption spectrophotometer. Fig. 13 shows the ZnO thin film's optical properties prior to and after the heat treatment at 500 ˚C. This reveals that the films have good quality with a sharp absorption edge. The absorption edges for the ZO-L1 and ZO-L7 are located at 360 and 370 nm respectively, which have shifted to 345 and 355 nm for the annealed samples. It is also noticeable after annealing at 500 ˚C shows maximum absorption of the thin films at a larger wavelength is higher because the surfaces became

homogenous and defects density decreased [62].

CONCLUSION

As from the above discussions and observations, the hexagonal wurtzite structure with a high degree of crystallinity was shown by the XRD pattern of synthesized ZnO nanoparticles along. Based on DLS results at a synthesis temperature of 150 ˚C, the average particle size for the synthesized ZnO nanoparticles was 60 nm. According to SEM characterizations of the deposited thin films, the voltage of 26 kV, the flow rate of 3 µl/min, and nozzle to substrate distance of 8 cm were observed as optimized deposition conditions. The ZnO nanoparticle's direct optical band gap was around 3.28 eV as shown by the UV visible absorption spectroscopy. In the wavelength larger than 345-350 nm, the maximum absorption of the annealed thin films has blue shifts because of the homogenous surface and low defect density.

CONFLICT OF INTEREST

The authors declare that there is no conflict of interests regarding the publication of this manuscript.

REFERENCES

1. Amakali T, Daniel LS, Uahengo V, Dzade NY, de Leeuw NH. Structural and Optical Properties of ZnO Thin Films Prepared by Molecular Precursor and Sol–Gel Methods. Crystals. 2020;10(2):132.
2. Munawar T, Mukhtar F, Yasmeen S, Naveed-ur-Rehman M, Nadeem MS, Riaz M, et al. Sunlight-induced photocatalytic degradation of various dyes and bacterial inactivation using CuO–MgO–ZnO nanocomposite. Environmental Science and Pollution Research. 2021;28(31):42243-42260.
3. Munawar T, Iqbal F, Yasmeen S, Mahmood K, Hussain A. Multi metal oxide NiO-CdO-ZnO nanocomposite–synthesis, structural, optical, electrical properties and enhanced sunlight driven photocatalytic activity. Ceram Int. 2020;46(2):2421-2437.
4. Nadeem MS, Munawar T, Mukhtar F, Naveed ur Rahman M, Riaz M, Hussain A, et al. Hydrothermally derived co, Ni co-doped ZnO nanorods; structural, optical, and morphological study. Opt Mater. 2021;111:110606.
5. Klingshirn CF, Meyer BK, Waag A, Hoffmann A, Geurts J. Zinc Oxide. Springer Series in Materials Science: Springer Berlin Heidelberg; 2010.
6. Bertolotti F, Tăbăcaru A, Muşat V, Ţigău N, Cervellino A, Masciocchi N, et al. Band Gap Narrowing in Silane-Grafted ZnO Nanocrystals. A Comprehensive Study by Wide-Angle X-ray Total Scattering Methods. The Journal of Physical Chemistry C. 2021;125(8):4806-4819.
7. Özgür Ü, Alivov YI, Liu C, Teke A, Reshchikov MA, Doğan S, et al. A comprehensive review of ZnO materials and devices. J Appl Phys. 2005;98(4):041301.
8. Abd-Elrahim AG, Chun D-M. Room-temperature deposition of ZnO-graphene nanocomposite hybrid photocatalysts for improved visible-light-driven degradation of methylene blue. Ceram Int. 2021;47(9):12812-12825.
9. Zu P, Tang ZK, Wong GKL, Kawasaki M, Ohtomo A, Koinuma H, et al. Ultraviolet spontaneous and stimulated emissions from ZnO microcrystallite thin films at room temperature. Solid State Commun. 1997;103(8):459-463.
10. Martínez MA, Herrero J, Gutiérrez MT. Deposition of transparent and conductive Al-doped ZnO thin films for photovoltaic solar cells. Sol Energy Mater Sol Cells. 1997;45(1):75-86.
11. Davis L. Properties of transparent conducting oxides deposited at room temperature. Thin Solid Films. 1993;236(1-2):1-5.
12. Schade H, Smith ZE. Optical properties and quantum efficiency of $Si_{1-x}C_x$: H/Si: H solar cells. J Appl Phys. 1985;57(2):568-574.
13. Jang JS, Kim J, Ghorpade U, Shin HH, Gang MG, Park SD, et al. Comparison study of ZnO-based quaternary TCO materials for photovoltaic application. J Alloys Compd. 2019;793:499-504.
14. Saha JK, Billah MM, Bukke RN, Kim YG, Mude NN, Siddik AB, et al. Highly Stable, Nanocrystalline, ZnO Thin-Film Transistor by Spray Pyrolysis Using High K Dielectric. IEEE Trans Electron Devices. 2020;67(3):1021-1026.
15. Cho J, Hwang S, Ko D-H, Chung S. Transparent ZnO Thin-Film Deposition by Spray Pyrolysis for High-Performance Metal-Oxide Field-Effect Transistors. Materials. 2019;12(20):3423.
16. Kim D, Yun I, Kim H. Fabrication of rough Al doped ZnO films deposited by low pressure chemical vapor deposition for high efficiency thin film solar cells. Current Applied Physics. 2010;10(3):S459-S462.
17. Carcia PF, McLean RS, Reilly MH, Nunes G. Transparent ZnO thin-film transistor fabricated by rf magnetron sputtering. Appl Phys Lett. 2003;82(7):1117-1119.
18. Graniel O, Fedorenko V, Viter R, Iatsunskyi I, Nowaczyk G, Weber M, et al. Optical properties of ZnO deposited by atomic layer deposition (ALD) on Si nanowires. Materials Science and Engineering: B. 2018;236-237:139-146.
19. Lu J, Chu J, Huang W, Ping Z. Preparation of Thick Pb(Zr, Ti)O_3(PZT) Film by Electrostatic Spray Deposition (ESD) for Application in Micro-System Technology. Jpn J Appl Phys. 2002;41(Part 1, No. 6B):4317-4320.
20. Ryu CK, Kim K. Fabrication of ZnO thin films using charged liquid cluster beam technique. Appl Phys Lett. 1995;67(22):3337-3339.
21. Joshi B, Samuel E, Kim Yi, Yarin AL, Swihart MT, Yoon SS. Electrostatically Sprayed Nanostructured Electrodes for Energy Conversion and Storage Devices. Adv Funct Mater. 2021;31(14):2008181.
22. Neagu R, Perednis D, Princivalle A, Djurado E. Initial Stages in Zirconia Coatings Using ESD. Chem Mater. 2005;17(4):902-910.
23. Gil Kim S, Hyun Choi K, Hwan Eun J, Joon Kim H, Seung Hwang C. Effects of additives on properties of MgO thin films by electrostatic spray deposition. Thin Solid Films. 2000;377-378:694-698.
24. Lee SC, Jeong J, Park HG, Min B-C, Chan Jun S, Chung KY. Binder-assisted electrostatic spray deposition of LiCoO2 and graphite films on coplanar interdigitated electrodes for flexible/wearable lithium-ion batteries. J Power Sources. 2020;472:228573.
25. Jiang W, Malshe AP, Brown WD. Physical powder deposition

of solid lubricant nanoparticles by electrostatic spray coating (ESC). Surf Coat Technol. 2004;177-178:671-675.
26. Li J, Fan H, Jia X, Chen J, Cao Z, Chen X. Electrostatic spray deposited polycrystalline zinc oxide films for ultraviolet luminescence device applications. J Alloys Compd. 2009;481(1-2):735-739.
27. Karimi M, Mirkazemi SM, Vahidshad Y, Javadpour J. Preparation and characterization of zinc sulfide thin film by electrostatic spray deposition of nano-colloid. Thin Solid Films. 2021;737:138929.
28. Jaworek A, Sobczyk AT. Electrospraying route to nanotechnology: An overview. J Electrostatics. 2008;66(3-4):197-219.
29. Sweet ML, Pestov D, Tepper GC, McLeskey JT. Electrospray aerosol deposition of water soluble polymer thin films. Appl Surf Sci. 2014;289:150-154.
30. Zhu C, Fu Y, Yu Y. Designed Nanoarchitectures by Electrostatic Spray Deposition for Energy Storage. Adv Mater. 2018;31(1):1803408.
31. Lee J, Koo H, Kim SY, Kim SJ, Lee W. Electrostatic spray deposition of chemochromic WO3-Pd sensor for hydrogen leakage detection at room temperature. Sensors Actuators B: Chem. 2021;327:128930.
32. Piner R, Li H, Kong X, Tao L, Kholmanov IN, Ji H, et al. Graphene Synthesis via Magnetic Inductive Heating of Copper Substrates. ACS Nano. 2013;7(9):7495-7499.
33. Hwang K-S, Jeong J-H, Jeon Y-S, Jeon K-O, Kim B-H. Electrostatic spray deposited ZnO thin films. Ceram Int. 2007;33(3):505-507.
34. Roncallo S, Painter JD, Ritchie SA, Cousins MA, Finnis MV, Rogers KD. Evaluation of different deposition conditions on thin films deposited by electrostatic spray deposition using a uniformity test. Thin Solid Films. 2010;518(17):4821-4827.
35. Ghimbeu CM, Schoonman J, Lumbreras M, Siadat M. Electrostatic spray deposited zinc oxide films for gas sensor applications. Appl Surf Sci. 2007;253(18):7483-7489.
36. Su B, Choy KL. Electrostatic assisted aerosol jet deposition of CdS, CdSe and ZnS thin films. Thin Solid Films. 2000;361-362:102-106.
37. Arce-Plaza A, Sánchez-Rodriguez F, Courel-Piedrahita M, Vigil Galán O, Hernandez-Calderon V, Ramirez-Velasco S, et al. CdTe Thin Films: Deposition Techniques and Applications. Coatings and Thin-Film Technologies: IntechOpen; 2019.
38. Dong H, Chen YC, Feldmann C. Polyol synthesis of nanoparticles: status and options regarding metals, oxides, chalcogenides, and non-metal elements. Green Chem. 2015;17(8):4107-4132.
39. Chen CH, Emond MHJ, Kelder EM, Meester B, Schoonman J. ELECTROSTATIC SOL–SPRAY DEPOSITION OF NANOSTRUCTURED CERAMIC THIN FILMS. J Aerosol Sci. 1999;30(7):959-967.
40. Mallikarjunaswamy C, Lakshmi Ranganatha V, Ramu R, Udayabhanu, Nagaraju G. Facile microwave-assisted green synthesis of ZnO nanoparticles: application to photodegradation, antibacterial and antioxidant. Journal of Materials Science: Materials in Electronics. 2019;31(2):1004-1021.
41. Shokry Hassan H, Elkady MF, El-Shazly AH, Bamufleh HS. Formulation of Synthesized Zinc Oxide Nanopowder into Hybrid Beads for Dye Separation. Journal of Nanomaterials. 2014;2014:1-14.
42. Anupama C, Kaphle A, Udayabhanu, Nagaraju G. Aegle marmelos assisted facile combustion synthesis of multifunctional ZnO nanoparticles: study of their photoluminescence, photo catalytic and antimicrobial activities. Journal of Materials Science: Materials in Electronics. 2017;29(5):4238-4249.
43. Holzwarth U, Gibson N. The Scherrer equation versus the 'Debye-Scherrer equation'. Nature Nanotechnology. 2011;6(9):534-534.
44. Sun Y, Xia Y. Shape-Controlled Synthesis of Gold and Silver Nanoparticles. Science. 2002;298(5601):2176-2179.
45. Eskandari M, Ahmadi V, Ahmadi SH. Low temperature synthesis of ZnO nanorods by using PVP and their characterization. Physica B: Condensed Matter. 2009;404(14-15):1924-1928.
46. Suliman AE, Tang Y, Xin Z, Jia Z. The Effect of PVP Addition and Heat-treatment Duration on Zinc Oxide Nanoparticles. Journal of Applied Sciences. 2006;6(6):1298-1301.
47. Al-Osta A, Alnehia A, Qaid AA, Al-Ahsab HT, Al-Sharabi A. Structural, morphological and optical properties of Cr doped ZnS nanoparticles prepared without any capping agent. Optik. 2020;214:164831.
48. Horn RG. Surface Forces and Their Action in Ceramic Materials. J Am Ceram Soc. 1990;73(5):1117-1135.
49. Yang Q. Gold Nanomaterials Bioconjugates. Chemistry of Bioconjugates: John Wiley & Sons, Inc.; 2014. p. 255-280.
50. Faisal S, Jan H, Shah SA, Shah S, Khan A, Akbar MT, et al. Green Synthesis of Zinc Oxide (ZnO) Nanoparticles Using Aqueous Fruit Extracts of Myristica fragrans: Their Characterizations and Biological and Environmental Applications. ACS Omega. 2021;6(14):9709-9722.
51. Modena MM, Rühle B, Burg TP, Wuttke S. Nanoparticle Characterization: Nanoparticle Characterization: What to Measure? (Adv. Mater. 32/2019). Adv Mater. 2019;31(32):1970226.
52. Guo Y-C, Cai C, Zhang Y-H. Observation of conformational changes in ethylene glycol–water complexes by FTIR–ATR spectroscopy and computational studies. AIP Advances. 2018;8(5):055308.
53. Saroj AL, Singh RK, Chandra S. Studies on polymer electrolyte poly(vinyl) pyrrolidone (PVP) complexed with ionic liquid: Effect of complexation on thermal stability, conductivity and relaxation behaviour. Materials Science and Engineering: B. 2013;178(4):231-238.
54. Rahma A, Munir MM, Khairurrijal, Prasetyo A, Suendo V, Rachmawati H. Intermolecular Interactions and the Release Pattern of Electrospun Curcumin-Polyvinyl(pyrrolidone) Fiber. Biological & Pharmaceutical Bulletin. 2016;39(2):163-173.
55. Muthukumaran S, Gopalakrishnan R. Structural, optical and photoluminescence studies of heavily Mn-doped ZnO nanoparticles annealed under Ar atmosphere. Journal of Materials Science: Materials in Electronics. 2011;23(7):1393-1401.
56. Lanje AS, Sharma SJ, Ningthoujam RS, Ahn JS, Pode RB. Low temperature dielectric studies of zinc oxide (ZnO) nanoparticles prepared by precipitation method. Adv Powder Technol. 2013;24(1):331-335.
57. Gliemann G. K. Nakamoto: Infrared and Raman Spectra of Inorganic and Coordination Compounds. John Wiley and Sons, New York, Chichester, Brisbane, Toronto 1978. 3. Aufl., XV, 448 Seiten mit 109 Abbildungen und 95 Tabellen. Preis: $ 31,15. Berichte der Bunsengesellschaft für physikalische Chemie. 1978;82(11):1263-1263.

58. Osuntokun J, Ajibade PA. Structural and Thermal Studies of ZnS and CdS Nanoparticles in Polymer Matrices. Journal of Nanomaterials. 2016;2016:1-14.
59. Gong X, Tang CY, Pan L, Hao Z, Tsui CP. Characterization of poly(vinyl alcohol) (PVA)/ZnO nanocomposites prepared by a one-pot method. Composites Part B: Engineering. 2014;60:144-149.
60. Maensiri S, Laokul P, Promarak V. Synthesis and optical properties of nanocrystalline ZnO powders by a simple method using zinc acetate dihydrate and poly(vinyl pyrrolidone). J Cryst Growth. 2006;289(1):102-106.
61. Lian J, Liang Y, Kwong F-l, Ding Z, Ng DHL. Template-free solvothermal synthesis of ZnO nanoparticles with controllable size and their size-dependent optical properties. Mater Lett. 2012;66(1):318-320.
62. Gao X, Li X, Yu W. Flowerlike ZnO Nanostructures via Hexamethylenetetramine-Assisted Thermolysis of Zinc–Ethylenediamine Complex. The Journal of Physical Chemistry B. 2005;109(3):1155-1161.